Published paper
Lawes, M., Lee, Y., Mokhtar, A.S. and Woolley, R. (2008) *Laser ignition of iso-octane air aerosols.* Combustion Science and Technology, 180 (2). pp. 296-313.

http://dx.doi.org/10.1080/00102200701739198

Laser ignition of iso-octane air aerosols

M. Lawes, Y. Lee, A. S. Mokhtar* and R. Woolley

School of Mechanical Engineering, University of Leeds, Leeds LS2 9JT, UK

*Department of Aerospace Engineering, Faculty of Engineering, Universiti Putra Malaysia, Malaysia

Corresponding author: Robert Woolley
Department of Mechanical Engineering,
University of Sheffield
Mappin Street
Sheffield
S1 3JD
UK

E mail Rob.Woolley@sheffield.ac.uk

Abstract

Iso-octane aerosols in air have been ignited with a focused Nd:YAG laser at pressures and temperatures of 100 kPa and 270 K and imaged using schlieren photography. The aerosol was generated using the Wilson cloud chamber technique. The droplet diameter, gas phase equivalence ratio and droplet number density were determined. The input laser energy and overall equivalence ratio were varied. For 270 mJ pulse energies initial breakdown occurred at a number of sites along the laser beam axis. From measurements of the shock wave velocity it was found that energy was not deposited into the sites evenly. At pulse energies of 32 mJ a single ignition site was observed. Overall fuel lean flames were observed to locally extinguish, however both stoichiometric and fuel rich flames were ignited. The minimum ignition energy was found to depend on the likelihood of a droplet existing at the focus of the laser beam.

1. Introduction

A number of practical combustion problems result from the difficulty of igniting premixed fuel-air mixtures. These include high altitude relight of gas turbines and cyclic variations in spark ignition reciprocating engines. Laser ignition has been proposed as a potential ignition source that can offer some advantages over conventional systems such as the ability to position the ignition source optimally for ignition, rather than for mounting or durability reasons (Ronney, 1994 and El-Rabii et al., 2004). A variety of laser ignition strategies are available and these include the use of: a high flux density from a focused pulsed laser to breakdown the fuel-air premixture (Spiglanin, 1995); a wavelength tuned laser to excite a specific species within a mixture (Lucas, 1987; Forch and Miziolek, 1991) or a laser beam that is focused onto a target thereby reducing the energy flux density required (Bach et al., 1969). To date, the first option appears to be the most practical, employing relatively simple and comparatively cheap laser systems and permitting the movement of the ignition position by steering the beam.

A large amount of work has been undertaken on the laser ignition of gas phase fuel-air premixtures for a variety of fuels that include hydrogen and methane (Spiglanin, 1995; Phuoc and White, 1999). Laser intensities of the order of 200 GW/cm^2 for air at 100 kPa and 300 K are required to generate a plasma in a gas (Bradley et al., 2004). The plasma is formed via the relatively inefficient process of multiphoton ionisation and inverse bremsstrahlung resulting in an electron cascade and then a plasma (Radziemski, 1989). Once the plasma is formed, laser ignition kernels propagate in a similar manner to those caused by electrical breakdown, with generation of a toriod which propagates normal to the direction of the laser beam (Kono, 1989). However, after approximately 50 μs the kernel begins to propagate along the axis and towards the incoming laser igniter. This results in laser ignition kernels having a distinctive ‘mushroom’ shape (Spiglanin et al., 1995).

In real combustion chambers the fuel is often introduced as a spray and the optimum ignition position may then be at the edge of the spray where a mixture of vapourised fuel, air and fuel droplets co-exist. A lot of work has been performed on the interaction between single droplets and focused laser beams, demonstrating the influence of the liquid and droplet size on the breakdown process (Chylek et al., 1987; Hsieh, 1987). It has been shown that the droplet acts like a lens and focuses the laser light with ignition occurring on the shadow side of the droplet in either the gas or liquid phase. Once breakdown has occurred, plasma is vented from the droplet away from the laser and

explosive vapourisation of the droplet occurs. Although the breakdown energy is a function of droplet and gas material and of droplet size, quoted intensities are typically of the order 0.5 GW/cm^2 for a 35 μm water droplet (Hsieh, 1987) and this is over two orders of magnitude smaller than for gas phase ignition. To date little work has been performed on the laser ignition of multiple droplets in sprays or droplet clouds, although El-Rabii et al. (2005) determined minimum ignition energies in well characterized droplet clouds. They demonstrated that they were lower than those for gas phase ignition.

In this study, aerosols of iso-octane were generated in a laminar cloud chamber. A very narrow range of droplet sizes existed and the gas phase equivalence ratio and droplet number density were known. The laser was focused into the centre of the chamber and successfully ignited the premixture. The influence of laser ignition energy and fuel/air equivalence ratio on the ignition kernel and subsequent flame development were investigated.

2. Experimental

Laser ignition unit

The ignition system consisted of a Nd:YAG laser (operating at 1064 nm, pulse duration 15 ns) and beam steering optics and is shown in Fig. 1. The energy of the laser beam was controlled with a halfwave plate, and Glan polariser and measured, in-situ, by a (wedge and photodiode) power meter. A x4 beam expander (Gallilean telescope) was employed to enlarge the beam to enable a tighter focus and a plano convex lens focused the beam at the centre of the vessel. The same system was used in a previous study on gas phase laser ignition (Bradley et al, 2004)

Explosion vessel and aerosol characteristics

Aerosol mixtures were generated in a combustion bomb by the Wilson cloud chamber technique (Wilson, 1911). This technique has been used previously in combustion studies by Hayashi (1976) and Lawes et al. (2006). Well defined, near mono-dispersed, droplet suspensions was generated with diameters that could be varied between 0 and 25 μm. The aerosols were generated in-situ by controlled expansion of a gaseous fuel-air mixture into an expansion vessel. The combustion vessel was a development of the one used by Abdel-Gayed et al., (1984). It comprised a 305 mm diameter by 305 mm long cylindrical bomb in which four fans, driven by 1.5 kW motors generated, when required, uniform and

isotropic turbulence within a central region of the vessel. Windows of 150 mm diameter were placed in both end plates to provide optical access for various laser diagnostics. Elevated temperatures could be obtained by the use of two electrical heaters attached to the inside walls of the bomb. A small side window was fitted for the laser ignition beam to enter.

The combustion and expansion vessels were evacuated then isolated from each other with a pneumatic valve. Iso-octane was then injected into the combustion vessel and evapourated. Dry air was allowed into the vessel to achieve the desired equivalence ratio and initial pressure. Complete evaporation and mixing was assured by preheating the vessel and running the fans. For the laminar measurements reported here, the fans were then stopped and the mixture allowed to settle. Immediately prior to ignition, the mixture in the combustion vessel was vented, at a controlled rate, lasting for up to 3 seconds through a 6 mm orifice into the expansion vessel. This caused a reduction in mixture pressure and temperature in the combustion vessel that took the mixture into the wet regime such that droplets were formed. Experimental variables, which include pressure, temperature, liquid and gaseous phase equivalence ratio, droplet diameter distribution and number density, were functions of initial pressure, temperature, rate of expansion and time from the start of expansion (Lawes, 2006). Two equivalence ratios are quoted: ϕ_{ov} which is the overall equivalence ratio based on the fuel/air mixture in the vessel before expansion and ϕ_g which is the gas phase equivalence ratio at the time of ignition and varies depending on the proportion of fuel in the liquid phase.

Shown in Fig. 2 are the conditions within the combustion vessel during the expansion of a stoichiometric mixture of iso-octane and air from an initial temperature and pressure of 303 K and 200 kPa. The temperature was measured with a fine wire (25 μm) type K thermocouple and the pressure was monitored using a pressure transducer.

The temporal variation of droplet mean diameter, D_{10} , was measured by Phase Doppler Anemometry, PDA, which comprised a 30 mW, LaserPhysics, Ar-ion laser, transmission and receiving optics and a Dantec signal processor, model 58N10. The length mean diameter, D_{10} , is given by

$$D_{10} = \frac{\sum_{i=1}^{k} (n_i D_i)}{\sum n_i} \qquad (1)$$

The results, shown as crosses in Fig 2, comprise data from seven locations within the central region of the vessel and were obtained from different experiments. The PDA system could not adequately detect droplets of less than about 2 μm. Therefore, the first measurements were recorded from approximately 1.4 s from the start of expansion. Over the next 3 s, the droplet diameter increased up to approximately 25 μm. Up to about 2.7 s, a narrow distribution of sizes was obtained, the standard deviation which was as low as 10 % of the mean diameter (Lawes et al., 2006). Hence the distribution was assumed to be near mono-dispersed. By igniting mixtures at different times following the start of expansion the droplet diameter during combustion could be varied. Because expansion, and hence temporal variation in droplet diameter, took place over a period of almost 3 seconds while ignition and combustion lasted a few microseconds and milliseconds respectively quasi steady state conditions could be assumed. In the present work all mixtures were ignited at 2.1 s from the start of expansion, resulting in a measured pressure and temperature at ignition of 112 ± 5 kPa and 265 ± 5 K. Selecting an alternative equivalence ratio resulted in a variation in the droplet size, Table 1.

It was not possible to obtain measurements of the droplet number density with PDA because of the small measurement volume and low data rate. Therefore, laser attenuation measurements were used, the results of which are shown in Fig. 2. The laser attenuation experiments were performed with a 10 mW, He-Ne laser which was expanded to a beam of 150 mm diameter and passed through the vessel and then focused onto photodiode to record the laser power through a number of expansions. The number density could be calculated using the Beer-Lambert Law (e.g. Chigier, 1991) which assuming a mono-dispersed droplet cloud and negligible multiple scattering predicts the attenuation of light from aerosols

$$I / I_o = \exp(-n \frac{\pi D^2}{4} Q_c(f, D) L) \qquad (2)$$

where, I/I_o is the normalised laser power intensity, Q_c is the attenuation efficiency which is the function of wave (laser) frequency, f, and droplet diameter D (obtained from the PDA measurements), and is constant for visible frequencies, and L is the optical path length taken to be 305 mm which is the length of the vessel. Once the number density and droplet sizes were known the gas phase equivalence ratios could be calculated and are

shown in Fig. 3. The number density increased rapidly reaching a maximum at 1.75 s from the start of expansion after which it remained effectively constant. The gas phase equivalence ratio decreased approximately linearly from 1.75 s onwards. Therefore from 1.75 to 2.5 s the droplet size was growing but no new droplets were created nor was there significant droplet agglomeration as there was no significant decrease in the number density .

Imaging system

High-speed pin-hole schlieren photography with a He-Ne laser light source was employed to visualise plasmas, shock waves and flames. A schematic is shown in Fig. 1. The beam was expanded by a microscope objective lens and passed through a 150 mm diameter collimating lens of 1000 focal length and projected on a frosted glass screen. An Imacon 468 ultra-high-speed electronic imaging system recorded the schlieren images. This camera could record a pre-programmed sequence of 8 images at different times between successive frames up to 100 MHz Typically, it was programmed to record the first four frames at a high framing rate to capture the shock wave, and the subsequent frames at a slower rate to capture flame development. Synchronisation between the camera and laser igniter was obtained by using the same triggering pulse to open the Q-switch on the ignition laser and the camera.

Typically 5 ignitions were performed at each condition. Sources of shot to shot variation include the: laser power, laser power distribution, droplet distribution at the focus and droplet size. The most critical sources of error were: getting the equivalence ratio correct, slight scatter in the pre expansion temperature (resulting in variation in the droplet diameter) and variation in the laser power. The consequences of the first two sources are a 15 % variation in the burnrate (Lawes et al, 2006) and a standard deviation scatter in the laser power.

3. Results and discussion

Table 1 gives a summary of all experiments and includes details of the fuel-air mixture, and delivered and deposited laser energies. Before droplet clouds were investigated, stoichiometric, gaseous, propane-air mixtures were ignited to observe the performance of the laser system. The resulting images of a ignition kernel of a 240 mJ laser pulse are shown in Fig. 4. The quoted laser energy was measured prior to the beam entering the aerosol, corrected for losses in the optics. In the case of aerosols the energy at the focus was less than this because the pulse energy was attenuated by the droplets prior to the focal point. The kernel developed as a classical ignition kernel with movement back

towards the laser after 100 μs generating a 'mushroom' shape (or third lobe) (Spiglanin, 1995). The centre of the ignition kernel at 100 μs was used to define the focal point of the ignition system.

Shown in Fig. 5 are schlieren images of the early stages of ignition kernel development resulting from a 170 mJ laser pulse for an overall stoichiometric areosol mixture. The first image, taken 5 μs after the Q-switch fired, shows 5 ignition sites (numbered 1 to 5 on the figure) distributed over 34 mm. The focus of the laser was in the centre of the image and, hence, site 4 occurred just after the focus. As the laser intensity required to breakdown a droplet is significantly less than that required for air it is assumed that each site corresponds to the laser induced breakdown of at least one droplet. Shock waves, of differing size can be seen to propagate from sites 2 to 5, the larger shock waves coming from sites 2 and 4. Progressively, all shock waves become less visible, the one at the largest site, 4, persisting the longest. Site 2 appears to be made up of three smaller sites, is non-spherical in shape and two of the three smaller ignition sites are off axis. A reason for these 'off axis' ignitions might be due to the larger diameter of the laser beam at this location, which is approximately 8 mm from the laser focal point, based on the position that a propane-air flame broke down. Another explanation could be multiple scattering between particles, leading to secondary ignitions.

Shockwave radii are shown in Fig. 6 for a number of shock fronts. Although laser ignition does not provide instantaneous energy input, and the initial plasma volume is finite, blast wave analysis is often applied to gas phase laser ignition with reasonable agreement (Spiglanin et al 1995 and Bradley et al., 2004). In the present work the estimated energy deposited in each ignition site, E, was found from measurements of the shock wave radius, r_s,. They are related by Taylor, (1950)

$$r_s = t^{2/5}\left(\frac{E}{\rho_o}\right)^{1/5} \tag{3}$$

Where t is time from the energy deposition and ρ_o, the gas density. Equation 3 was applied to the shockwaves from sites 4 and 5 in Fig. 5 and fitted to the experimental shock wave at 8 μs. The resulting predictions using Eq. 3 are shown as dashed lines in Fig. 6. Also shown is the shockwave radius for a gas phase ignition, (E = 224 mJ, for the same ignition system, from Bradley et al. (2004)) which is consistently larger than those

measured here. The energies deposited in sites 4 and 5 was calculated to be 65 and 9 mJ respectively; thus over 7 times more energy was deposited within the larger ignition kernel. Considering 4 of the 5 ignition sites in Fig. 5 (in the case of site 1, no shock wave was detected and the kernel did not grow over the observed period, therefore the energy deposited was neglected): site 2 had a similar shock wave size to site 4 and site 3 is similar to site 5. By addition the deposited energy was approximately 150 mJ, which was of the same order as the measured energy input. However comparison between the experimental shockwave radius and Eq. 3 can be seen to be poor. This was probably due to the nature of the energy deposition which was not instantaneous but was finite (Bradley et al., 2004).

Ignition kernel development at similar conditions to those in Fig. 5 (although at a higher laser power), but imaged over a longer duration of 2.5 *ms* is shown in Fig. 7. For this, a longer exposure time was used compared with the images in Fig 5 in order to improve image quality, but as a result the shock wave was not visible. In this case, twelve ignition sites, along the laser beam axis, were evident at 8 ns after Q switching and these were centred, approximately, at the focus of the laser beam. The number of ignition sites changed with each experiment and are thought to be a function of local variations in both the droplets and laser pulse. The mean spacing between ignition sites was 2.4 mm. Towards the laser beam, at the left of the images, the ignition centres tended to occur off axis. The kernel size did not change over the first 20 μs. However, by 40 μs the ignition sites had clearly started to merge. The two ignition kernels to the right of the images, furthest from the laser, preferentially grew along the axis away from the laser. By 2.5 ms the flame kernel had developed into a central region with a wrinkled flame surface, with two 'fingers' growing outwards along the axis with a smooth flame surface.

Shown in Fig. 8 are kernel images for an overall equivalence ratio, ϕ_{ov}, of 0.75, the leanest equivalence that could be successfully ignited with a 240 mJ laser pulse. In the early stages, the kernel appeared to be similar to that in Fig. 7, for ϕ_{ov} = 1.0, with 12 ignition sites along the axis of the ignition laser, although the mean spacing between kernels was slightly smaller at 2 mm. After 3 ms, the flame kernel appeared, superficially, like a gas phase laser ignition kernel, Fig 4, having expanded radially out from the laser focus and also towards the laser. The ignition sites to the right of the focus quenched before 3 *ms*. Between 3 and 11 ms the kernel did not substantially grow. The flame surface was highly wrinkled, having the appearance of a turbulent flame. The edge of the schlieren image

was less distinct than at richer equivalence ratios, possibly due to increased flame thickness and some local flame extinction. For both ϕ_{ov} = 1.0 and ϕ_{ov} = 0.75 the ignition kernels appeared almost turbulent, similar highly wrinkled flame surfaces have been observed across fuel lean gas phase laser ignition kernels (Bradley et al. 2004). The flame chemistry may not have had sufficient time to establish a self propagating front, in which case the schlieren images are showing the hydrodynamic front resulting from the rapid expansion of hot gases at ignition. Therefore the wrinkling could reflect the density/energy variations at the breakdown. Parts of the ignition kernel were also observed to have a smooth surface (e.g. the two fingers at a far left and right in Fig. 8) these are thought to be the result the formation of a induced flow similar to that of the third lobe seem in gas phase ignition. How the induced flow is setup in this situation (with the presence of the droplets) is not known, and further experiments would be required to observe in detail the ignition process in individual droplets and the interaction between adjacent ignition centres.

Images of the ignition of a fuel rich mixture at ϕ_{ov} = 1.4, are shown in Fig. 9 for a 240 mJ laser pulse. Here, the aerosol was denser than in the previous images resulting in greater attenuation of the laser beam, and fewer ignition sites, typically 8 with a mean spacing of 2.6 mm. At 20 μs, the size of the ignition sites increased towards the right of the image, at increasing distance from the incident laser. By 2 ms the kernel had grown at a normal to the laser axis and had a roughly cylindrical shape. To the right of the image (away from the laser) there was a V shaped indentation observable in the schlieren image pointing towards the laser. This phenomenon has been observed in laser induced fluorescence images of gas phase laser ignition kernels and is caused by an induced flow into the kernel towards the incident laser beam (Spiglanin, 1995). The induced flow is the consequence of the generation of relatively strong toroid due to axis symmetric deposition of the laser. Why this feature, which is associated gas phase ignition, also occurs in droplet ignition is not evident. The flame surface was again wrinkled although it is believed that at this rich ϕ this is due to the onset of a cellular laminar instability. This mixture was observed to be cellular by Lawes et al (2006) with spark ignition, they showed that laminar aerosol flames became cellular at lower pressures and smaller radii than observed in gaseous flames.

The images discussed above were obtained with laser energies considerably above the required minimum. In the present work, the lowest laser energy that resulted in ignition

(at ϕ_{ov} = 1.0) was 32 mJ, schlieren images of the ignition are shown in Fig. 10. Between 80 ns and 20 μs from Q-switching, only a single ignition kernel was observed whose size remained constant. By 3 ms a classical laser ignition kernel was evident with toroidal growth normal to the axis and on-axis propagation towards the laser (Spiglanin, 1995). The same overall flame shape remained for the next 8 ms. By 15 ms the flame kernel had attained a roughly spherical shape. With a mixture at ϕ_{ov} = 1.4, shown in Fig. 11, the ignition again only occurred at a single point. However, in this case the kernel adopted toroidal shape similar tho that observed in electrical sparks, rather than in laser ignition as seen in Fig. 10. Ultimately, a spherical flame ball developed, which appeared to be cellular (like that of Fig. 9, the same mixture but larger ignition energy). The onset of cellularity is primarily a function of the response of a flame to stretch and curvature and depends on the relative importance of thermal and species diffusion (Bradley et al. 2000), and hence, is strongly dependent on ϕ. Whilst the onset of the cellularity might be influenced by the ignition source, rich gaseous iso-octane flames have been observed to be cellular from ignition at elevated pressures (Bradley et al. 2000) and aerosols at atmospheric pressure (Lawes et al, 2006).

Kernel cross sectional areas plotted against time are shown in Fig. 12 for a laser energy of 240 mJ and Fig. 13 for an energy of 32 mJ. The kernels were imaged in the early stages just after the laser pulse (μs) and later (ms) when the plasma had given way to a deflagration. There was significant scatter in the measurements, this is thought to be a result of the interaction between the laser and the droplets, with different numbers of droplets acting as centres in each ignition. El-Rabii (2005) found strong shot to shot variations in minimum ignition energy measurements in droplet clouds with incident laser energies known with good precision. In the early stages (upto 200 μs) in Fig. 12 the kernel area was did growth at any of the three equivalence ratios. However the leanest kernels (ϕ_{ov} = 0.75) were generally larger than those for the richer mixtures. This may be because more ignition sites were observed under lean conditions due to the cloud being less dense hence more energy was available at ignition. However, later in the flame growth the fuel rich kernels were larger than either the stoichiometric or lean flames. This would be expected as the laminar burning velocity for the gas phase equivalence ratio (ϕ_g = 1.1) is close to the maximum. The time taken for the kernels to reach an (arbitrary) area of 1500 mm^2 is shown in Table 1. The ϕ_{ov} = 1.4 reached 1500 mm^2 in the shortest time, the stoichiometric flame took twice the time and the lean flame was an order of magnitude

greater. Also shown in Fig. 12 is the area of gas phase stoichiometric propane-air ignition kernel, in the early stages its area was less than those of the gas phase results but by a millisecond its area was similar in magnitude to those of aerosol ignitions. Shown in Fig 13 are the areas for the 32 mJ energy ignitions, the high energy gas phase ignition is also shown, as a reference. Although in the earlier stages their area is much smaller than the higher ignition energy cases (as there was only a single ignition source) they achieve an area of 1500 mm^2 in only twice the time of the stoichiometric high energy case, and in a much shorter time than the high energy lean kernels. Stoichiometric and fuel rich flames (which were cellular) would be expected to propagate faster than lean equivalence ratios once ignition is finished and the flame chemistry dominates (Lawes et al, 2006).

Approximate laser intensities were determined from calculated spot diameters, however these are subject to error as they depend on lens aberrations, temporal and spatial laser pulse variations and in this case the effect of the droplet cloud. The laser energy at the focus, E_{focus}, was estimated using the Beer-Lambert Law, Eq. 2, the results are shown in Table 1. The droplet number density and diameter were obtained from the calibration experiments presented in Figs. 2 and 3. It was assumed that the attenuation of the focused 1064 nm laser beam could be treated in a similar manner to that for a 632 nm He-Ne beam and beam broadening from Mie scattering was neglected The laser focal spot diameter was calculated using (Steen, 1998):

$$d_f = \frac{4 f \lambda M^2}{\pi d_b} \tag{4}$$

where

$$M^2 = 0.25\, d_i\, \theta / \lambda \tag{5}$$

Here df is the focal point diameter (mm), d_i the initial laser beam diameter (mm), d_b the expanded laser beam diameter (mm), f the focal length of the focusing lens (mm), λ the wavelength of laser light (nm), θ the beam divergence (rad), and M^2 the beam quality factor. For a laser beam of 6 mm diameter, $\lambda = 1064$ nm, and $\theta = 0.8$ mrad, then $M^2 = 3.54$. With the optical configuration adopted, the value of df from Eq. (4) was 0.061 mm. Laser intensities were calculated at the focus and are shown in Table 1. The variation of the beam diameter with axial distance, x, from the focal point, $d(x)$, is given by Steen (1998)

$$d(x) = d_f \sqrt{1+\left(\frac{4M^2 x\lambda}{\pi d_f^2}\right)^2} . \quad (6)$$

Using Eq. (6) the laser intensity along the axial direction was determined and is shown in Fig. 14 for laser beams of 240 and 32 mJ (the intensity is affected by the laser attenuation due to droplet prior to the focus, which is a function of ϕ_{ov}). As the number density of droplets was known, the number of particles, n_{focus}, present within the ignition volume could also be found. The length of the ignition volume was measured from the images and was taken to be the length over which droplets were observed to break down. In the case of an input energy of 240 mJ, an ignition length of 32 mm was used and many more particles (of order 600) were within the ignition volume than were observed to ignite by the laser. For the low energy ignitions, breakdown was found to occur within 1 mm of the focus and the number of particles present was calculated to be just less than 1. The minimum ignition energy was therefore limited by the likelihood of particle being present within the focal volume. The calculated laser intensities, G_{focus} at the focus were much larger than the minimum breakdown values determined for single droplets, which are typically of the order 0.5 GW/cm^2 (Hsieh, 1987). However, the intensity rapidly fell away from the focus. The furthest point from the focus at which droplets were observed to breakdown was approximately 0.2 GW/cm^2. This is of the same order as the minimum intensity for droplet breakdown reported in (Hsieh, 1987). However, for the lower laser ignition energy of 32 mJ breakdown only appeared to take place at relatively high intensities ≈ 5 GW/cm^2. Therefore the breakdown process may not have been as efficient as reported in the single droplet studies, the beam attenuation process more efficient than calculated or there was error in the attenuation calculations. Nevertheless it can be concluded that the likelihood of breakdown depends on the number of droplets in the control volume.

Conclusions

Iso-octane-air aerosols have been successful ignited in a combustion bomb operated as a cloud chamber under laminar conditions. The operating conditions were well characterised and droplet size, number density and gaseous equivalence ratio known. Measurements were performed for mixtures at range of equivalence ratios and for two laser energies of 240 and 32 mJ. In the case of 240 mJ, multiple ignitions occurred along

the axis of the laser beam, resulting in a single long (approximately 36 mm) ignition kernel. From observations of the shock waves it was concluded that energy deposited within the ignition sites varied. The length of the ignition kernel was set by their being sufficient laser intensity to breakdown a droplet. Qualitative differences were observed between ignitions at overall lean, stoichiometric and rich mixtures. The relatively large size of the ignition kernel is likely to make this as an effective method of ignition as gas phase ignition.

For 32 mJ pulse energies, a single ignition point occurred close to the focus of the laser beam. In the case of an overall stoichiometric mixture a classical three lobed ignition kernel and for rich mixtures a spherical flame ball were observed. Analysis of the laser intensity at the focus found qualitatively that the minimum ignition energy was controlled by the likelihood of the particle being present at the focus.

References

Abdel-Gayed R.G., Al-Khishali K.J. and Bradley D. (1984) Turbulent burning velocities and flame straining in explosions. *Proc. R. Soc., Lond. A,* **391,** 393-414.

Bach G. G., Knystautas, R. and Lee J. H. (1969) *Proc. Combust. Instit.,* **12**, 853.

Bradley, D; Sheppard, C G W; Woolley, R; Greenhalgh, D A and Lockett, R D. (2000) The development and structure of flame instabilities and cellularity at low Markstein numbers *Combust. Flame* **122**, 195-209.

Bradley D., Sheppard C.G.W., Suardjaja I.M., and Woolley, R. (2004) Fundamentals of high-energy spark ignition with lasers. *Combust. Flame*, **138**, 55–77.

Chigier N., (1991) *Combustion Measurements*, Hemisphere.

Chylek P., Jarzembski M.A., Srivastava V., Pinnick R.G., Pendleton J.D., and Cruncleton J.P. (1987) Effect of spherical-particles on laser-induced breakdown of gases. *Applied Optics*, 26(5), 760-762.

El-Rabii H., Zähringer k., Rolon J.-C. and Lacas, F. (2004) Laser ignition in a lean premixed prevaporized injector, *Combust. Sci. Tech*., **176**: 1391-1417,

El-Rabii H., Gaborel G., Lapios J.-P., Thévenin, D., Rolon J.-C. and Martin J.-P. (2005) Laser spark ignition of two-phase monodisperse mixtures. *Optics Com.*, **256**, 495–506.

Forch, B.E. and Miziolek, A. W. (1991) Laser-based ignition of H_2/O_2 and D_2/O_2 premixed gases through resonant multiphoton excitation of H and D atoms near 243 nm**.** *Combust. Flame,* **85**, 254.

Hayashi, S., Kumagai, S., Sakai, T., (1976), *Combust. Sci. Tech.,* **15**, 169.

Hsieh W.-F., Eickmans J.H., and Chang R.K. (1987) Internal and external laser-induced avalanche breakdown of single droplets in an argon atmosphere. *J. Opt. Soc. Am. B,* **4**, 1816.

Kono M., Niu K., Tsukamoto T. and Ujiie Y. (1989) *Proc. Combus Instit.,* **22**, 1643.

Lawes, M., Lee Y., and Marquez, N. (2006) Comparison of iso-octane burning rates between single-phase and two-phase combustion for small droplets. *Combust. Flame*, **144**, 513–525

Lucas D., Dunn-Rankin D., Hom, K. and Brown, N. J. (1987) Ignition by excimer laser photolysis of ozone. *Combust, Flame,* **69**, 171.

Nishioka, M. and Law, C.K. (1997) A numerical study of ignition in the supersonic hydrogen-air laminar mixing layer. *Combust. Flame*, **108**, 199–219.

Phuoc T.X. and White F.P. (1999) Laser-induced spark ignition of CH_4/air mixtures. *Combust. and Flame,* **119**, 203.

Radziemski L. J. and Cremers D. A., (1989) *Laser-Induced Plasmas and Applications*, Marcel Dekker, New York.

Spiglanin T.A., McIlroy A., Fournier E.W., Cohen R.B., Syage J.A. (1995) Time-resolved imaging of flame kernels: Laser spark ignition of H_2/O_2/Ar mixtures. *Combust. Flame,* **102**, 310.

Steen W. M., (1998) *Laser Material Processing*, Springer-Verlag, London.

Ronney, P. (1994) Laser versus conventional ignition of flames. *Opt. Eng*., **33**, 510–521.

Taylor G.I., (1950), The Formation of a blast wave by a very intense explosion 1. theoretical, *Proc. R. Soc., Lond. A,* **201**, 159-174.

Wilson C.T.R. (1911), On a method of making visible the paths of ionising particles through a gas, *Proc. R. Soc., Lond. A,* **85**, 285-288.

Table 1 Details of the fuel-air mixture, and delivered and deposited laser energies.

ϕ_{ov}	E, mJ	D_{10}, μm	E_{focus}, mJ	n_{focus}	G_{focus}, $GW\ cm^{-2}$	*t, s
0.75	240	17.4	110	625	693	1.4×10^{-2}
1.0	240	17	110	528	604	3.0×10^{-3}
1.4	240	24.2	110	475	546	1.3×10^{-3}
1.0	32	17	13	0.8	71	6.2×10^{-3}
1.4	32	24.2	13	0.7	65	6.2×10^{-3}
**1.0	240					1.7×10^{-3}

* Time taken, t, to reach an area of 1500 mm^2

** gas phase propane air ignition.

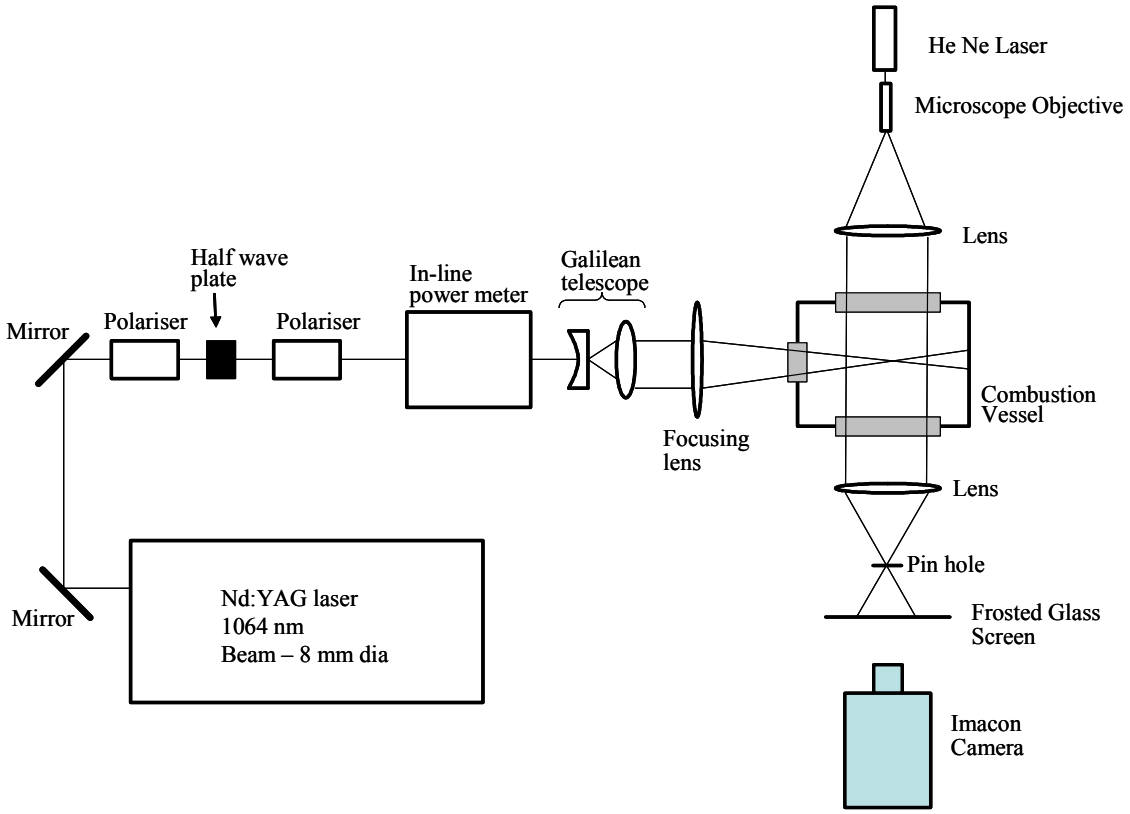

Fig. 1 A schematic of the experimental setup.

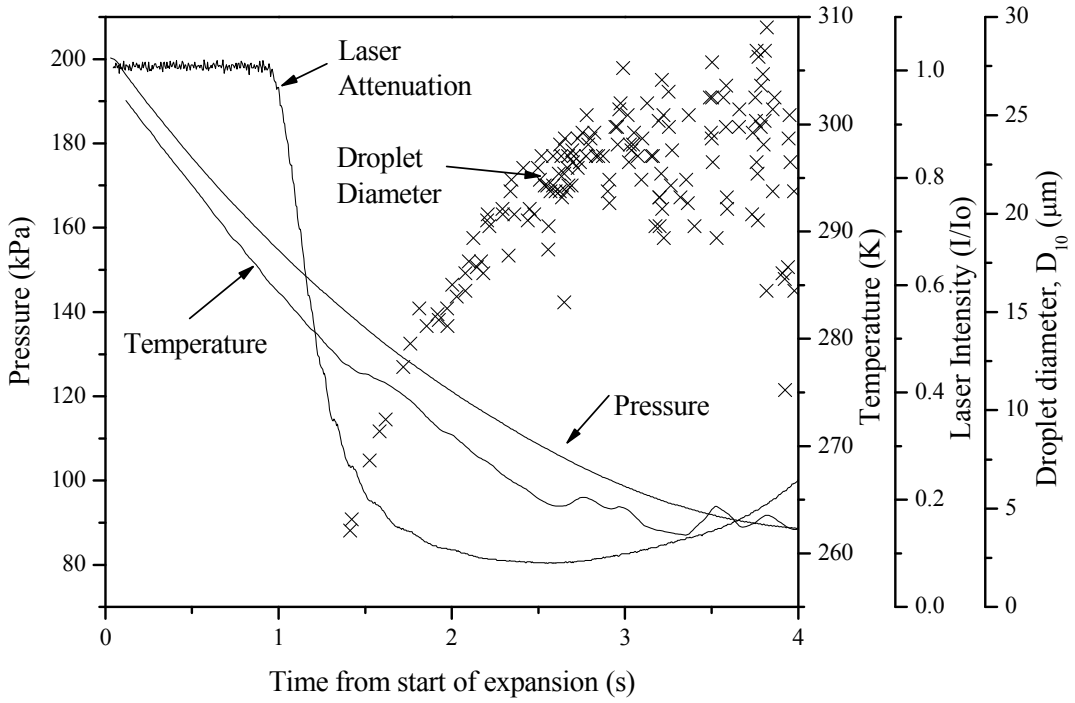

Fig. 2. Variation of temperature, pressure, laser intensity and droplet diameter, D_{10}, with time from start of expansion from an initial pressure and temperature of 200 kPa and 303 K.

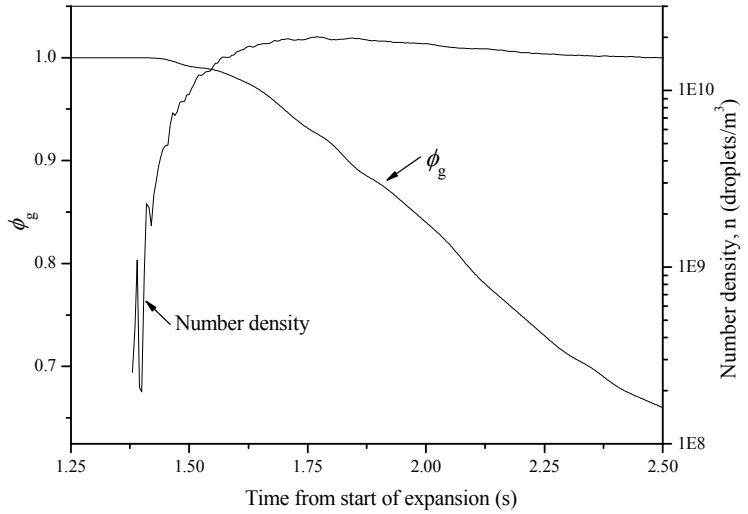

Fig. 3. Variation of calculated gas phase equivalence ratio and droplet number density with time during the expansion of stoichiometric iso-octane-air mixtures from an initial pressure and temperature of 200 kPa and 303 K.

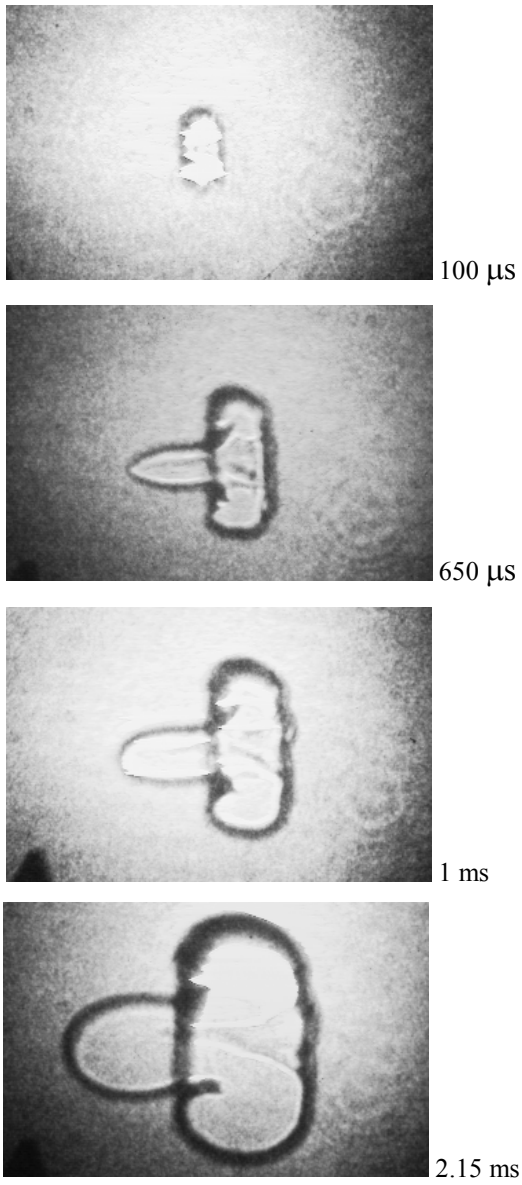

Fig. 4. Schlieren images showing ignition kernel development, propane-air, ϕ = 1.0, 100 kPa, 308 K, E = 240 mJ. Laser from left to right. Images at stated times after Q switch. Image length = 36 mm.

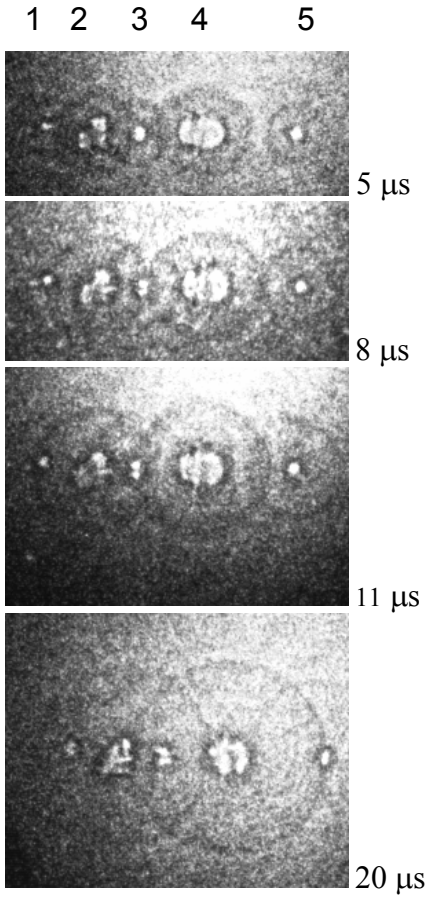

Fig. 5. Schlieren images showing ignition kernel development $\phi_{ov} = 1.0$, $\phi_g = 0.8$, 100 kPa, 270 *K*, E = 170 mJ. Laser from left to right. Images at stated times after Q switch. Image length = 36 mm.

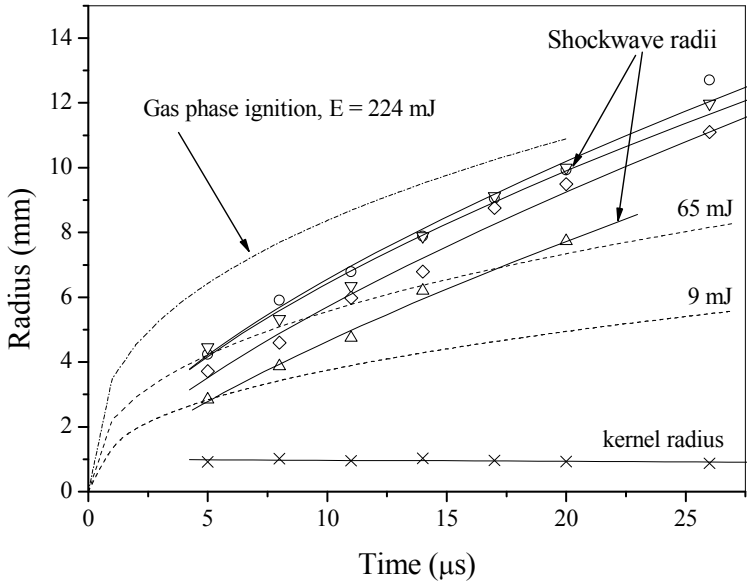

Fig. 6 Shockwave radius with time from ignition for $\phi_{ov} = 1.0$, $\phi_g = 0.8$, 100 kPa, 270 K. Dashed lines, shockwave radius predicted by Eq. 5, for the energies indicated. Dash dotted line, shockwave radius of gas phase laser ignition from Bradley et al., 2004.

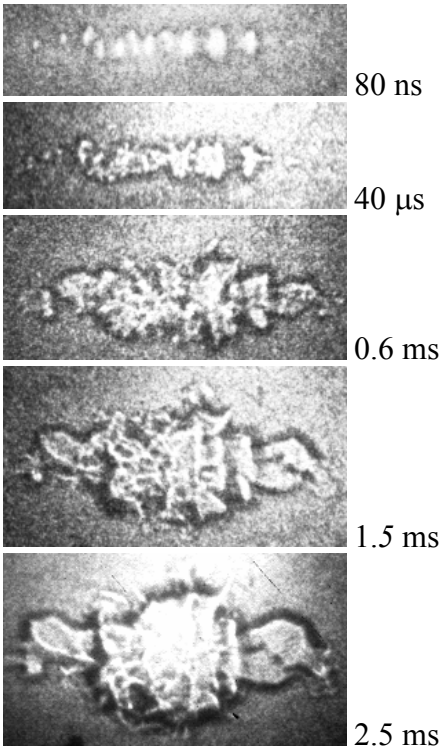

Fig. 7. Schlieren images showing ignition kernel development $\phi_{ov} = 1.0$, $\phi_g = 0.8$, 100 kPa, 270 K, E = 240 mJ. Image length = 44 mm.

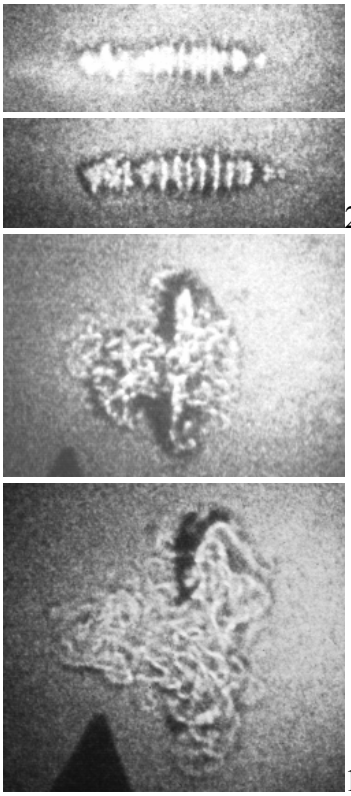

Fig. 8. Schlieren images showing ignition kernel development $\phi_{ov} = 0.7$, $\phi_g = 0.6$, 100 kPa, 270 K, E = 240 mJ. Image length = 44 mm.

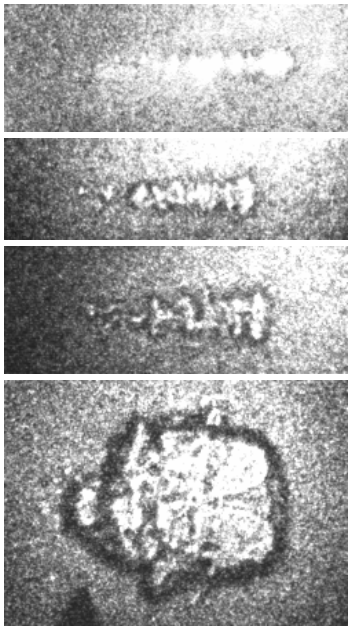

Fig. 9. Schlieren images showing ignition kernel development $\phi_{ov} = 1.4$, $\phi_g = 1.1$, 100 kPa, 270 K, E = 240 mJ. Image length 44 mm.

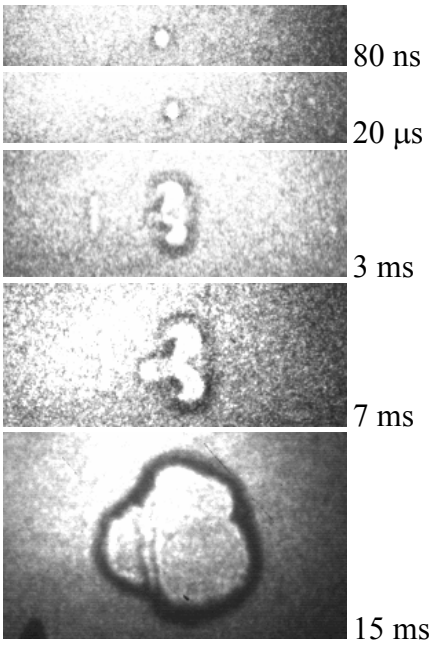

Fig. 10. Schlieren images showing ignition kernel development ϕ_{ov} = 1.0, ϕ_g = 0.8, 100 kPa, 270 K, E = 32 mJ. Image length = 35 mm.

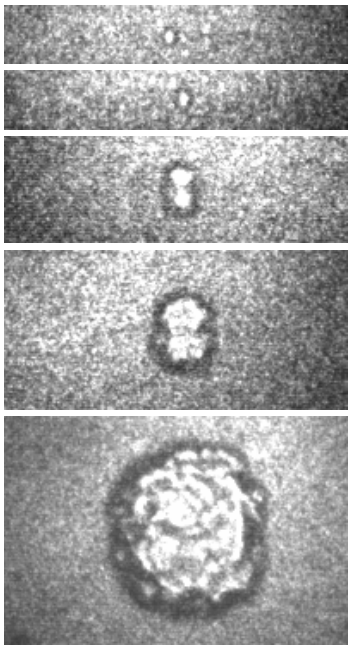

Figure 11. Schlieren images showing ignition kernel development $\phi_{ov} = 1.4$, $\phi_g = 1.1$, 100 kPa, 270 K, E = 32 mJ. Image length = 35 mm.

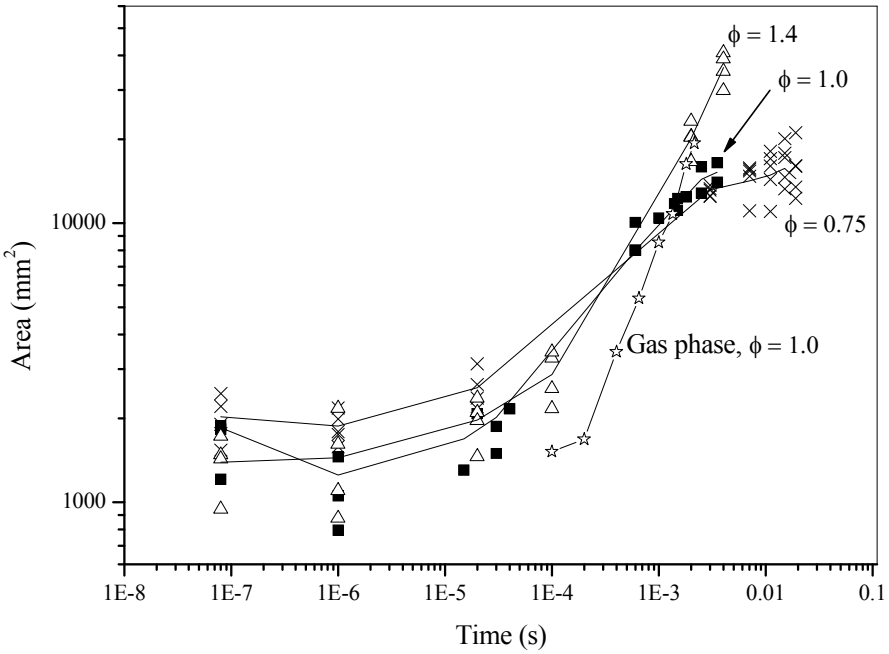

Figure 12. Kernel/flame area with time from ignition, for a 240 mJ laser pulse.

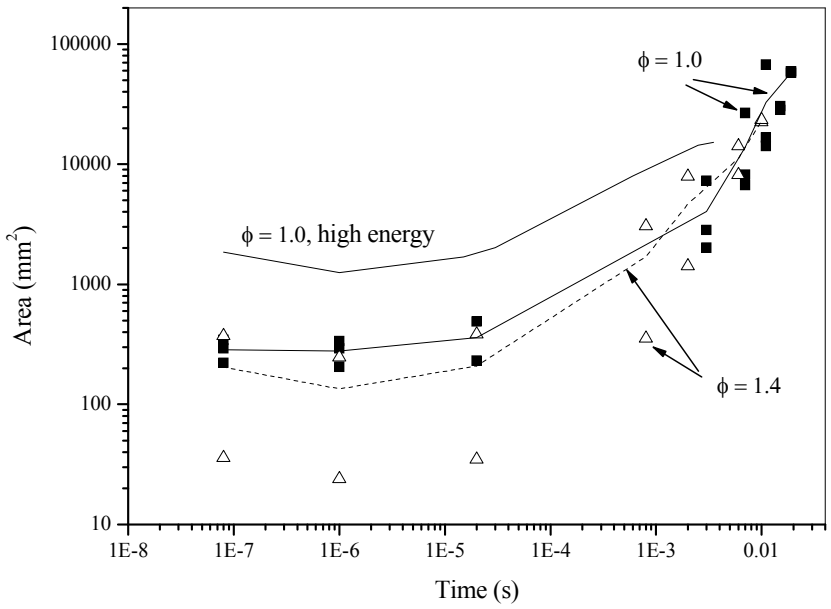

Figure 13. Kernel/flame area with time from ignition, for a 32 mJ laser pulse.

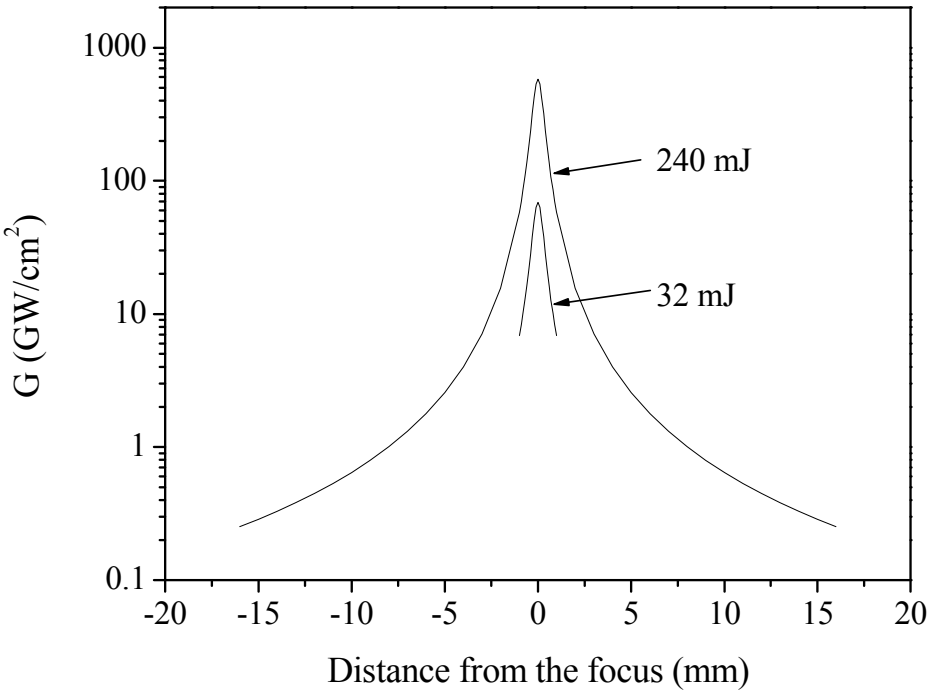

Figure 14. Calculated laser intensity with distance form the focus for a 240 and 32 mJ laser beam, $\phi_{ov} = 1.0$.